On Low-Pass, High-Pass, Bandpass, and Stop-Band NGD RF Passive Circuits

B. Ravelo

Normandy University, UNIROUEN, ESIGELEC IRSEEM EA 4353
Technopole du Madrillet, Avenue Galilée
BP 10024
F-76801 Saint Etienne du Rouvray, France
E-mail: blaise.ravelo@yahoo.fr

Abstract

The negative group delay (NGD) function is one of the most intriguing phenomena that can be encountered in area of physics. Since the first experiments in the early 1980s, this abnormal phenomenon remains unfamiliar to conventional engineering. Based on physical, analytical, and experimental investigations, it was found that the NGD phenomenon corresponds to the advanced effect of a pulse signal at baseband frequency. This paper introduces the basic understanding of this extraordinary phenomenon. The RF and microwave-circuit theory dedicated to NGD passive circuits based on the *S*-parameter modeling is established. Two general types of lumped-element-based RF passive topologies, constituted of simple parallel and series mounted impedances, are explored. Low-pass, high-pass, bandpass, and stop-band elementary topologies of passive cells are treated and characterized. The low-pass NGD cells are first-order passive circuits consisting of *RL*-series mounted in parallel and *RC*-parallel networks mounted in series. The different steps of the circuit-parameter calculations as functions of the expected NGD level, insertion loss, and reflection coefficient are explained. To validate the theory, proofs-of-concept (POC) of NGD passive circuits were synthesized, designed, and simulated. As predicted in theory, the simulation results confirmed the feasibility of the low-pass, high-pass, bandpass, and stop-band NGD functions. The NGD circuits respected the basic criteria of RF and microwave circuits with reflection coefficients better than −12 dB. Despite the attenuation, the simulated low-pass NGD cell presented an NGD level of about −1 ns and a cutoff frequency equal to 46 MHz. The high-pass NGD cell presented a group-delay frequency response opposite to the low-pass NGD cell. The bandpass NGD cell exhibited an NGD level of about −2 ns at the center frequency of 0.5 GHz, and a bandwidth of about 92 MHz. Furthermore, the counterintuitive time-advance effect, induced by the NGD phenomenon, proven with various arbitrary-waveform baseband signals, was observed. A pulse advancement of about −1 ns was obtained with the considered low-pass passive cell.

1. Introduction

In the 1970s, an analytical investigation of the propagation of a Gaussian light pulse through an anomalous dispersion medium with negative refractive index was reported by Garrett and McCumber [1]. This theoretical result enabled understanding the negative group delay (NGD) effect in the time domain. After this theoretical conceptualization, the first experiments on NGD were performed in 1982 by Chu and Wong [2]. This experimental demonstration was based on the atomic-vapor medium, and showed the NGD phenomenon at optical wavelengths. However, several physicists remained skeptical about the existence of the NGD phenomenon. The NGD phenomenon was therefore assumed to typically be artifacts of numerical calculations, and not a real physical phenomenon. Consequently, this unfamiliar phenomenon was not sufficiently developed and less interesting to scientists, researchers, and engineers over the 1980s.

Despite this period of low interest, a new era of NGD functionality blew in with the 1990s with the unbelievable demonstrations with basic electronic circuits composed of familiar electronic components such as resistances, inductances, and capacitors. One decade after the first NGD demonstration by Chu and Wong, the first experiments with lumped electronic circuits was performed by the team of Chiao [3-6]. The NGD circuit topology was identified from an analogy between the atomic-vapor medium and the electronic-circuit's transfer function [3, 4]. Theoretical and experimental studies were then conducted with active optical systems [7-9] and electronic systems operating with audio signals [10-12] in order to illustrate the existence of the NGD phenomenon. During this period, one of the NGD effect's basic meanings was explained by electronic experiments considering pulse-shaped voltage signals with millisecond duration. It was visualized that the output pulse's leading and trailing edges occurred before the input pulse had completely penetrated into the NGD circuit. It was emphasized that this counterintuitive NGD phenomenon did

not contradict the causality effect [5, 6, 10, 11]. However, at this stage, the complexity and operational speed limitations linked to the operational amplifiers did not motivate the electronic design engineers to exploit the NGD concept.

Some years later, the NGD phenomenon was synthesized with microwave and millimeter-wave circuits that were able to operate at higher frequencies [13-15]. In the same period, the NGD phenomenon was also generated with metamaterial microwave circuits, especially those based on periodic transmission-line structures [16-18]. Based on the microwave design and analyses, it was found that the NGD effect was generally generated with circuits that were typically lossy and resonate [13-24]. The NGD effect appeared around the resonance frequency. However, it was understood from time-domain experiments that this counterintuitive NGD effect was systematically accompanied with significant losses [18, 19]. This combined effect was inherently linked to the absorption around the resonance frequency. Because of the signification loss, there was little interest in the NGD concept during several decades.

To tackle this technical problem, microwave circuit topologies, based on the field-effect transistor (FET) and the low-noise amplifier (LNA), were proposed [25-28]. An analytical methodology enabling identification of simple NGD active microwave topologies was elaborated [26]. Several basic elementary NGD topologies susceptible to generating the NGD function were identified. A generalized NGD circuit theory was introduced. It was emphasized that the NGD function was similar to linear filter gain [29]. Low-pass, high-pass, bandpass, and stop-band NGD cells were identified. It was reported that the low- and high-pass NGD cells were typically first-order linear circuits.

An innovative *RC*-network-based high-pass NGD circuit was introduced in [30]. The bandpass and stop-band elementary cells were based on second-order resonating circuits. The NGD circuit's fundamental properties, such as the NGD level, the NGD cutoff frequencies, the NGD bandwidth, and the NGD figure-of-merit (FoM) were established and described. NGD circuit theory has been made widely available with the testing of several basic and elementary circuits. The feasibility of the theoretical concept has been validated by simulations and experiments. NGD effects have been simultaneously generated with the possibility of gain and loss compensation. Despite these developments in NGD circuit-design methodology, it was emphasized that the NGD effect does not allow any time-advance configuration because of its inherent properties [31].

In addition to NGD design and synthesis, potential applications – notably, *RC*-interconnection propagation delay [32] cancellation – have been forecasted since the 2000s [33, 34]. The feasibility of this delay cancellation was later extended to signal recovery for signal-integrity enhancement, as suggested in [35-37]. Further potential NGD applications for high-performance feed-forward amplifier design were also proposed [38].

Despite this trend of NGD theory becoming widely available, RF and electronic engineers are still not familiar with the NGD function. Further illustration is therefore needed for the NGD function to achieve further understanding in the academic and industrial points of view. In the present paper, we address a simple theoretical approach making it easy to understand the NGD function with lumped passive elementary cells. The aim of the paper is to make the NGD concept familiar to electrical-engineering students, researchers, and those in industry. The present paper is also aimed at making the NGD concept and theory as familiar as possible to the non-specialist. In doing this – based on the analogy between NGD and filter theory [29] – the low-pass, high-pass, bandpass, and stop-band elementary lumped *RC* cells are investigated. This microwave circuit theory is developed from particularly simple low-pass topologies of lumped-element components consisting of an *RL* series network and an *RC* parallel network. These act as first-order circuits that can be investigated in a manner similar to any familiar electrical function. A theoretical approach based on the *S*-parameter analysis is introduced in Section 2. The theory also presents the basic NGD properties and synthesis methodology for the basic NGD cells. By considering the familiar, known low-pass-to-bandpass circuit transformation in filter theory, bandpass NGD cells are also then investigated. The validity of the proposed NGD theory, simulations, and experimental results is presented and explored in Section 3. Both frequency- and time-domain analyses are deployed in order to show the NGD phenomena. Moreover, the ability to tune the NGD function level of the circuit parameters is tested for the deep understanding about the ability to control the NGD function with the lumped-circuit parameters. The conclusion of the paper is then presented in Section 4.

2. Generality of the Passive Topologies Under Study

The present section is focused on a simple way to design low-pass and bandpass NGD circuits, based on the familiar electronic components *R*, *L*, and *C*. After exploring the NGD effect's existence with two passive lumped-element-based topologies, we will investigate the *S*-parameter modeling methodology. The theoretical characterization of the active circuit obtained will then be described. At the end of each step, synthesis expressions enabling one to easily calculate the NGD circuit parameters as a function of the NGD specifications will be formulated.

2.1 Introduction to Basic Topology

The present subsection generally describes the elementary passive topologies of the circuit to be developed in this paper.

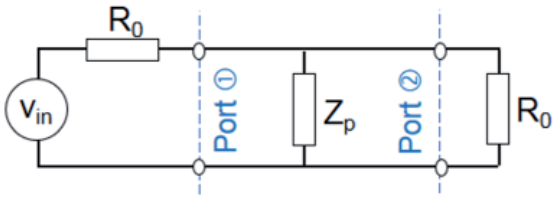

Figure 1. A shunt-impedance Z_p type passive topology.

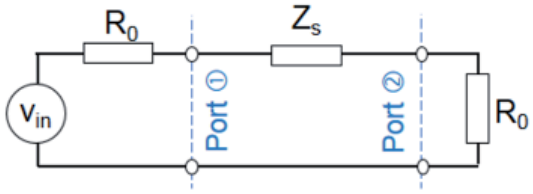

Figure 2. A series-impedance Z_s type passive topology.

Similar to all classical electronic and electrical circuits, the simplest and elementary topologies are based on the two-port circuit as a simple impedance that can be denoted *Z*. As pointed out in [25, 26, 29], we can start our investigation with a simple two-port circuit composed of a parallel impedance, Z_p, as depicted in Figure 1, or a series impedance, Z_s, as depicted in Figure 2. It should be underlined that in this paper, R_0 represents the reference impedance, equal to 50 Ω.

The present study is based on this two-port circuit *S*-parameter analysis. For the case of passive topologies, the associated *S* parameters can be defined by the symmetric relationship

$$[S]=\begin{bmatrix} S_{11} & S_{12} \\ S_{21} & S_{22} \end{bmatrix}. \tag{1}$$

2.2 *S*-Parameter Modeling

The present subsection describes the *S*-parameter modeling of the passive cells introduced in Figure 1 and Figure 2 of the previous subsections. The constituting element impedances, $Z_p(j\omega)$ and $Z_s(j\omega)$, are assumed to depend on the angular frequency, ω. After the determination of branch currents and applying the definition of the *S* parameters, we get the following expressions:

For the parallel-impedance-based cell:

$$\left[S_p(j\omega)\right]=\begin{bmatrix} \dfrac{-R_0}{R_0+2Z_p(j\omega)} & \dfrac{2Z_p(j\omega)}{R_0+2Z_p(j\omega)} \\ \dfrac{2Z_p(j\omega)}{R_0+2Z_p(j\omega)} & \dfrac{-R_0}{R_0+2Z_p(j\omega)} \end{bmatrix}, \tag{2}$$

For the series-impedance-based cell:

$$\left[S_s(j\omega)\right]=\begin{bmatrix} \dfrac{Z_s(j\omega)}{2R_0+Z_s(j\omega)} & \dfrac{2R_0}{2R_0+Z_s(j\omega)} \\ \dfrac{2R_0}{2R_0+Z_s(j\omega)} & \dfrac{Z_s(j\omega)}{2R_0+Z_s(j\omega)} \end{bmatrix}. \tag{3}$$

It can be emphasized that the reflection and transmission coefficients of these passive circuits are linked by the relationship

$$S_{11}(j\omega)+S_{21}(j\omega)=1. \tag{4}$$

This means that the circuit must generate significant insertion and reflection losses.

2.3 NGD Circuit Theory

Differently from the classical RF/microwave circuit theory, the unfamiliar NGD circuit theory is based on the sign of the group-delay analysis.

2.3.1 NGD Theoretical Analysis and Similarity to Filter Behavior

By denoting by $j\omega$ the circuit angular-frequency variable, according to circuit and system theory, it can be recalled that the group delay is defined by

$$\tau(\omega)=-\frac{\partial\varphi(\omega)}{\partial\omega}, \tag{5}$$

with

$$\varphi(\omega)=\angle S_{21}(j\omega), \tag{6}$$

Table 1. A comparison of the magnitude and group delay of NGD functions and conventional normal filters.

Characteristics	Normal Filter	NGD Function
Basic specifications	Transfer function gain	Transfer function group delay
Cutoff frequencies ω_c	Root of the equation $\lvert S_{21}(j\omega_c)\rvert = \lvert S_{21}(j\omega)\rvert_{\max}/\sqrt{2}$	Root of the equation $\tau(\omega_c)=0$
Bandwidth	$\lvert S_{21}(j\omega_c)\rvert \geq \lvert S_{21}(j\omega)\rvert_{\max}/\sqrt{2}$	$\tau(\omega)\leq 0$
Low-pass with bandwidth defined by $\omega \leq \omega_c$	In the bandwidth, we have $\lvert S_{21}(j\omega_c)\rvert \geq \lvert S_{21}(j\omega)\rvert_{\max}/\sqrt{2}$	In the bandwidth, we have $\tau(\omega)\leq 0$ and $\lvert S_{21}(j\omega)\rvert$ should be as flat as possible.
High-pass with bandwidth defined by $\omega \geq \omega_c$		
Bandpass with bandwidth defined by $\omega_{c_1} \leq \omega \leq \omega_{c_2}$		
Stop-band with bandwidth defined by $\omega \leq \omega_{c_1}$ and $\omega \geq \omega_{c_2}$		

being the transmission phase, expressed in radians. This last expression explains that our impedance cannot be a frequency-independent component, such as a simple resistance. In other words, to generate nonzero group delay, a reactive-element-based circuit is necessary.

It is worth noting that the group delay behaves similarly to the filter gain [29]. The NGD bandwidth corresponds to the frequency band where the group delay $\tau(\omega)<0$. The cutoff angular frequency, ω_c, is analytically the root of the equation $\tau(\omega_c)=0$. We can identify different types of group-delay cells. We have:

- A low-pass NGD function when the group delay is negative, $\tau(\omega)<0$, in the lower frequency band, $\omega \leq \omega_c$ or from $\omega \approx 0$ to the cutoff angular frequency, ω_c.
- A high-pass NGD when the group delay is negative, $\tau(\omega)<0$, in the upper frequency band, $\omega \geq \omega_c$.
- A bandpass NGD when the group delay is negative, $\tau(\omega)<0$, in the frequency band $\omega_{c_1} \leq \omega \leq \omega_{c_2}$ by supposing $\tau(\omega_{c_1})=\tau(\omega_{c_2})=0$. In this case, the NGD central frequency, ω_0, can be verified with

$$\tau(\omega_0)=\min\left[\tau(\omega)\right]<0. \tag{7}$$

The NGD bandwidth can respectively be written as

$$\Delta\omega=\omega_{c_2}-\omega_{c_1}. \tag{8}$$

- A stop-band NGD when the group delay is negative, $\tau(\omega)<0$, in the frequency band $\omega \leq \omega_{c_1} \cup \omega_{c_2} \leq \omega$ by supposing $\tau(\omega_{c_1})=\tau(\omega_{c_2})=0$.

The performance of the passive NGD circuit can be evaluated with the figure-of-merit (FoM) defined by

$$FoM_{low-pass}=\lvert S_{21}(\omega\approx 0)\rvert\,\tau(\omega\approx 0)\,\omega_c \tag{9}$$

$$FoM_{band-pass}=\lvert S_{21}(\omega\approx\omega_0)\rvert\,\tau(\omega=\omega_0)\,\Delta\omega. \tag{10}$$

The better is the NGD circuit, the higher is the figure-of-merit.

2.3.2 A Comparison Between NGD Functions and Normal Conventional Filters

Despite the previous definitions of the NGD function types, one may wonder or be confused about the NGD and classical-filter aspects. Table 1 provides a comparative illustration between NGD functions and conventional normal filters. Based on circuit theory, the conventional normal filter's bandwidths are defined where the transmission gain's magnitude satisfies the equation $\lvert S_{21}(j\omega)\rvert \geq \lvert S_{21}(j\omega)\rvert_{\max}/\sqrt{2}$. As previously described, the NGD functions are mainly based on the sign of the group delay.

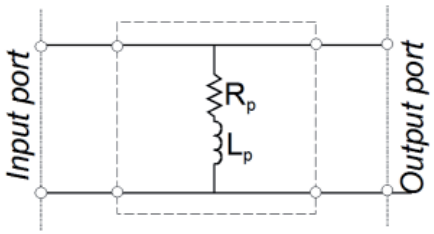

Figure 3. A low-pass NGD cell: *RL*-series shunt network.

2.3.3 Low-Pass NGD Passive Circuit Synthesis Method

Based on RF/microwave engineering, the main circuit parameters are basically the access matching and the insertion loss for passive circuits. Those parameters are still under consideration in the present study. However, in addition, we also deal with the group delay defined in Equation (5). For the low-pass NGD circuit, the NGD characterization described in this section is mainly obtained from the analytical expression of the *S* parameters and the group delay at very low frequencies, when $\omega \approx 0$. The synthesis method consists of the calculation of the NGD circuit's parameters as a function of the specified NGD level $\tau(\omega \approx 0) = \tau_0 < 0$, which is inversely linked to the NGD bandwidth; the insertion loss; and the reflection coefficients. In other words, the basic relations can be summarized in the following system:

$$\begin{cases} |S_{11}(\omega \approx 0)| = s_{11} \\ |S_{21}(\omega \approx 0)| = s_{21} \\ |S_{22}(\omega \approx 0)| = s_{11} \\ \tau(\omega \approx 0) = \tau_0 \end{cases}. \tag{11}$$

3. Shunt-Impedance-Type Elementary NGD Cells

The present section is focused on the NGD characterization of the family of shunt-impedance-type elementary NGD cell shown in Figure 1. Based on classical circuit theory, the simplest network configurations constituting the shunt impedance Z_p must be first-order circuits. This intuitive analysis leads us to consider *RL* and *RC* networks to build a low-pass NGD cell that will be analyzed in the present section.

3.1 Low-Pass Cell

The analytical identification performed in [26] stated that the only configuration of first-order or low-pass NGD circuits associated with the parallel impedance configuration is an *RL*-series network:

$$Z_p(j\omega) = R_p + j\omega L_p . \tag{12}$$

The low-pass NGD elementary cell is depicted in Figure 3.

3.1.1 Frequency-Dependent *S* Parameters and Group Delay

For the shunt-impedance-based low-pass NGD cell, the *S* parameters can be rewritten as follows:

$$[S_p(j\omega)] = \begin{bmatrix} \dfrac{-R_0}{R_0 + 2(R_p + j\omega L_p)} & \dfrac{2(R_p + j\omega L_p)}{R_0 + 2(R_p + j\omega L_p)} \\ \dfrac{2(R_p + j\omega L_p)}{R_0 + 2(R_p + j\omega L_p)} & \dfrac{-R_0}{R_0 + 2(R_p + j\omega L_p)} \end{bmatrix} \tag{13}$$

From this we can determine the following reflection- and transmission-coefficient magnitudes:

$$|S_{p11}(j\omega)| = \left| \frac{-R_0}{R_0 + 2(R_p + j\omega L_p)} \right| \Rightarrow S_{p11}(\omega)$$

$$= S_{p22}(\omega) = \frac{2\sqrt{R_0^2}}{\sqrt{(R_0 + 2R_p)^2 + (L_p\omega)^2}} \tag{14}$$

$$|S_{p21}(j\omega)| = \left| \frac{2(R_p + j\omega L_p)}{R_0 + 2(R_p + j\omega L_p)} \right| \Rightarrow S_{p21}(\omega)$$

$$= S_{p12}(\omega) = \frac{2\sqrt{R_p^2 + (L_p\omega)^2}}{\sqrt{(R_0 + 2R_p)^2 + (L_p\omega)^2}} .$$

The associated transmission phase is given by

$$\varphi_p(\omega) = \arctan\left(\frac{L_p\omega}{R_p}\right) - \arctan\left(\frac{2L_p\omega}{R_0 + 2R_p}\right). \tag{15}$$

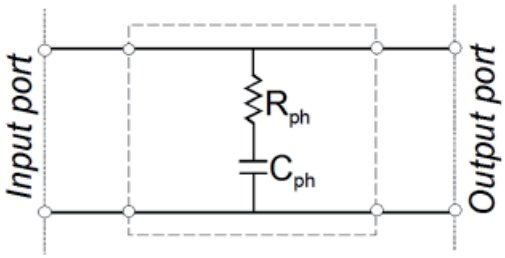

Figure 4. A high-pass NGD cell: *RC*-series shunt network family of the cell shown in Figure 3.

From the group delay defined in Equation (5), we have

$$\tau_p(\omega)=\frac{R_0L_p\left[2\left(L_p\omega\right)^2-R_p\left(R_0+2R_p\right)\right]}{\left[\left(L_p\omega\right)^2+R_p^2\right]\left[\left(2L_p\omega\right)^2+\left(R_0+2R_p\right)^2\right]} \quad (16)$$

3.1.2 NGD Characterization

At very low frequencies, the *S* parameters of the parallel-impedance-based circuit become

$$\left[S_p(\omega\approx 0)\right]=\begin{bmatrix}\frac{-R_0}{R_0+2R_p} & \frac{2R_p}{R_0+2R_p}\\ \frac{2R_p}{R_0+2R_p} & \frac{-R_0}{R_0+2R_p}\end{bmatrix}. \quad (17)$$

The associated group delay is given by

$$\tau_p(\omega\approx 0)=\frac{-R_0L_p}{R_p(R_0+2R_p)}. \quad (18)$$

It can be understood from the previous expression in Equation (18) that the passive cell introduced in Figure 3 behaves as a low-pass NGD circuit. In addition to the previous characteristics, one of the most important properties of the NGD cell is the NGD cutoff frequency, which can be denoted ω_{c_p}. It is the root of the equation $\tau_p\left(\omega_{c_p}\right)=0$. The proposed shunt-impedance-based low-pass NGD cell cutoff frequency is given by

$$\omega_{c_p}=\frac{\sqrt{R_p\left(R_0+2R_p\right)}}{\sqrt{2}L_p}. \quad (19)$$

The NGD figure-of-merit is expressed as

$$FoM_{low-pass_p}=\frac{-R_0^2}{\left(R_0+2R_p\right)\sqrt{2R_p\left(R_0+2R_p\right)}}. \quad (20)$$

It can be emphasized that the figure-of-merit is inversely proportional to the resistance R_p.

3.1.3 NGD Synthesis Method

Suppose we are given the desired insertion loss, *a*, the reflection coefficient, *r*, and the group delay, $\tau_0<0$. Analytically, the synthesis formulas are generated from Equation (18). After some calculations, we obtain the expressions for R_p and L_p associated with the shunt *RL*-series cell. The synthesis relations for this low-pass NGD cell are

$$\begin{cases} R_p(S_{11})=R_p(S_{22})=\frac{1-r}{2r}R_0 \\ \text{or} \\ R_p(S_{12})=R_p(S_{21})=\frac{a}{2(1-a)}R_0 \end{cases}, \quad (21)$$

$$\begin{cases} L_p(\tau_0)=-\left(1+\frac{2R_p}{R_0}\right)R_p\tau_0 \\ \text{or} \\ L_p(\omega_c)=\frac{\sqrt{R_p\left(R_0+2R_p\right)}}{\sqrt{2}\omega_c} \end{cases}. \quad (22)$$

3.2 High-Pass NGD Elementary Cells

The high-pass NGD cell family of the circuit proposed in Figure 3 is depicted in Figure 4.

Similarly to filter theory, the high-pass NGD cells can be easily synthesized from the low-pass cells via the low-pass-to-high-pass transform. As illustrated in Figure 4, the constitute shunt impedance can be expressed as

$$Z_{ph}(j\omega)=R_{ph}+\frac{1}{j\omega C_{ph}}. \quad (23)$$

The present subsection is focused on the NGD characteristics of the bandpass NGD cells associated with the previous cells.

3.2.1 High-Pass NGD Behavior

The *S* parameters of the series-impedance-based cell shown in Figure 4 become

$$\left[S_{ph}(j\omega)\right]$$

$$= \begin{bmatrix} \dfrac{j\omega R_0 C_{ph}}{2+j\omega C_{ph}\left(R_0+2R_{ph}\right)} & \dfrac{2\left(1+2j\omega R_{ph}C_{ph}\right)}{2+j\omega C_{ph}\left(R_0+2R_{ph}\right)} \\ \dfrac{2\left(1+2j\omega R_{ph}C_{ph}\right)}{2+j\omega C_{ph}\left(R_0+2R_{ph}\right)} & \dfrac{j\omega R_0 C_{ph}}{2+j\omega C_{ph}\left(R_0+2R_{ph}\right)} \end{bmatrix} \quad (24)$$

Similar to the low-pass-to-high-pass filter transform, the resistance element is not changed: $R_{ph} = R_p$. The associated group delay is given by

$$\tau_{ph}(\omega \approx 0) = \frac{R_0 C_{ph}}{2}. \quad (25)$$

In addition to the previous characteristics, one of the most important properties of the NGD cell is the NGD cutoff frequency, which can be denoted ω_{c_h}. This is the root of the equation $\tau_{ph}\left(\omega_{c_h}\right) = 0$. The proposed shunt-impedance-based high-pass NGD cell cutoff frequency is given by

$$\omega_{c_{ph}} = \frac{\sqrt{2}}{C_{ph}\sqrt{R_p\left(R_0+2R_p\right)}}. \quad (26)$$

Moreover, it is also found that for any integer $n > 1$, the group delay can be expressed as

$$\tau_{ph}\left(\omega = n\omega_{c_{ph}}\right)$$

$$= \frac{\left(1-n^2\right)R_0 R_p C_{ph}\left(R_0+2R_p\right)}{\left[R_0+2\left(1+n^2\right)R_p\right]\left[n^2 R_0+2\left(1+n^2\right)R_p\right]}. \quad (27)$$

It can be understood from the expressions in Equations (25), $\tau_{ph}(\omega \approx 0) > 0$, and (27), $\tau_{ph}\left(\omega = n\omega_{c_{ph}}\right) < 0$, which generally means that $\tau_{ph}\left(\omega > \omega_{c_{ph}}\right) < 0$. This means that the passive cell introduced in Figure 8 behaves as a high-pass NGD circuit. The NGD figure-of-merit is expressed as $FoM_{high-pass_p} = FoM_{low-pass_p}$. It can be emphasized that the figure-of-merit is inversely proportional to the resistance R_p.

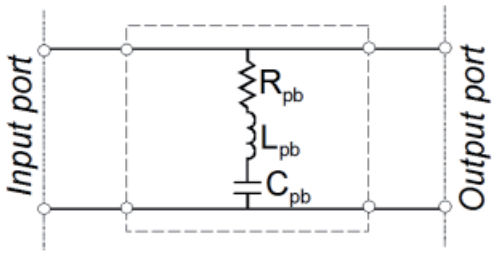

Figure 5. A bandpass NGD cell: *RLC*-series shunt network associated with the elementary cell shown in Figure 3.

3.2.2 Synthesis Method

For the high-pass NGD cell, the resistance parameter $R_{ph} = R_p$ can be synthesized with the relations in Equation (21). However, given the targeted positive group delay $\tau_0 > 0$, the capacitor C_{ph} can be extracted from the high-pass group delay expressed in Equation (25):

$$C_{ph} = \frac{2\tau_0}{R_0}. \quad (28)$$

This high-pass NGD cell capacitor can also be determined from the cutoff frequency expressed in Equation (26):

$$C_{ph} = \frac{\sqrt{2}}{\omega_{c_{ph}}\sqrt{R_p\left(R_0+2R_p\right)}}. \quad (29)$$

3.3 Bandpass NGD Elementary Cells

Similarly to filter theory, the bandpass NGD cells can be easily synthesized from low-pass cells via the low-pass-to-band-pass transform. The present subsection is focused on the NGD characteristics of the bandpass NGD cells associated with the previous cells. In this case, to synthesize the associated bandpass NGD cell, we just need to replace the inductance L_p by an *LC* series network, as shown in Figure 5. Based on filter-circuit theory, during the low-pass-to-bandpass transform, the resistance element is not changed: $R_{pb} = R_p$.

3.3.1 Bandpass NGD Behavior

The proposed cell's resonance frequency, which is also the NGD central frequency, is defined by

$$\omega_0 = \frac{1}{\sqrt{L_{ss}C_s}}. \quad (30)$$

The associated S parameters at the center frequency are expressed as

$$\left[S_{pb}(\omega_0)\right] = \left[S_p(0)\right] = \begin{bmatrix} \frac{-R_0}{R_0+2R_p} & \frac{2R_p}{R_0+2R_p} \\ \frac{2R_p}{R_0+2R_p} & \frac{-R_0}{R_0+2R_p} \end{bmatrix} \quad (31)$$

It can be demonstrated that the associated group delay is

$$\tau_{pb}(\omega_0) = 2\tau_p(0) = \frac{-2R_0L_{pb}}{R_p\left(R_0+2R_p\right)}. \quad (32)$$

This group delay is always negative around the resonance frequency.

3.3.2 Bandpass NGD Characterization and Properties

The NGD center frequency of the passive cell shown in Figure 5 is equal to $\omega = \omega_0$. The NGD bandwidth is defined by

$$\Delta\omega_{c_{pb}} = 2\omega_{c_p} = \frac{\sqrt{2R_p\left(R_0+2R_p\right)}}{L_{pb}}. \quad (33)$$

This means that the NGD cutoff frequencies are defined by

$$\omega_{c_{pb}} = \omega_0 \pm \omega_{c_p} = \frac{1}{\sqrt{L_{pb}C_{pb}}} \pm \frac{\sqrt{R_p(R_0+2R_p)}}{\sqrt{2}L_{pb}} \quad (34)$$

The NGD figure-of-merit is expressed as

$$FoM_{band-pass_p} = 2FoM_{low-pass_p}, \quad (35)$$

which is inversely proportional to the resistance, R_p.

3.3.3 Synthesis Method

The bandpass NGD cell synthesis relationships can be inspired from the low-pass relationships defined in Equations (21) and (22). To achieve the same NGD level, the resistance can be obtained from the same relationship and half of the inductance $L_{ph} = L_p$, which must be considered based on the group delay defined in Equation (32). The associated capacitor can be calculated from the inductance and the expected NGD center angular frequency, which can be denoted ω_0. We therefore have the capacitor-synthesis formula

$$C_{pb} = \frac{1}{\omega_0^2 L_{pb}}. \quad (36)$$

3.4 Stop-Band NGD Elementary Cells

Similarly to filter theory, the stop-band NGD cells can be easily synthesized from the low-pass cells via the low-pass-to-stop-band transform. Figure 6 represents the configuration of the stop-band cell associated with the circuit shown in Figure 3. Similarly to the low-pass-to-stop-band filter transform, the resistance element is not changed, $R_{ps} = R_p$. The present subsection is focused on the NGD characteristics of the bandpass NGD cells associated with the previous cells.

3.4.1 Stop-Band NGD Behavior, Characterization, and Properties

It can be demonstrated that the associated group delay is

$$\tau_{ps}(\omega_0) = R_0C_{ps}. \quad (37)$$

This group delay is always positive around the resonance frequency. The proposed shunt-impedance-based stop-band NGD cell cutoff frequencies are given by

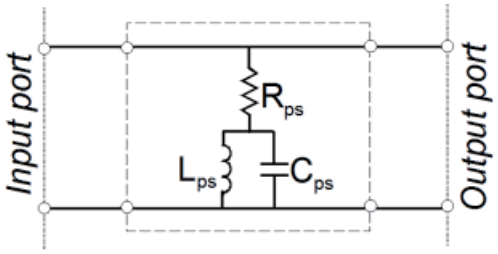

Figure 6. A stop-band NGD cell: R and LC-parallel series shunt network associated with the cell shown in Figure 3.

$$\omega_{c_{ps}} = \frac{1}{\sqrt{L_{ps}C_{ps}}} \pm \frac{\sqrt{2}}{C_{ps}\sqrt{R_{ps}\left(R_0 + 2R_{ps}\right)}}. \quad (38)$$

This means that the NGD bandwidths are

$$\begin{cases} \omega \le \dfrac{1}{\sqrt{L_{ps}C_{ps}}} - \dfrac{\sqrt{2}}{C_{ps}\sqrt{R_{ps}\left(R_0 + 2R_{ps}\right)}} \\ \text{and} \\ \omega \le \dfrac{1}{\sqrt{L_{ps}C_{ps}}} + \dfrac{\sqrt{2}}{C_{ps}\sqrt{R_{ps}\left(R_0 + 2R_{ps}\right)}} \end{cases} \quad (39)$$

For the case of a stop-band cell, the figure-of-merit cannot be defined.

3.4.3 Synthesis Method

The stop-pass NGD cell-synthesis relationships can be inspired from the combination of both low-pass and high-pass relationships. To obtain the attenuation, a, or the reflection coefficient, r, the resistance can be determined from the formula defined in Equation (21). For the given group delay, $\tau_0 > 0$, at the center angular frequency, which can be denoted ω_0, the capacitor can be calculated with the relationship in Equation (28), $C_{ps} = C_{ph}$. The associated inductance can be calculated from the inductance and the expected NGD center angular frequency, which can be denoted ω_0. We therefore have the inductance-synthesis formula

$$L_{ps} = \frac{1}{\omega_0^2 C_{ph}}. \quad (40)$$

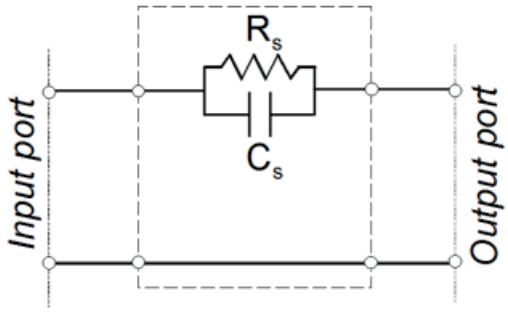

Figure 7. A low-pass NGD cell: *RC*-parallel series network.

4. Series Impedance-Type NGD Passive Cells

Similarly to the study performed in the previous section, the present section is focused on the NGD characterization of the family of series-impedance-type of elementary NGD topology shown in Figure 2. After checking different configurations, the first-order *RC*-parallel network constitutes the simplest cell to generate the low-pass NGD function.

4.1 Low-Pass NGD Elementary Cell

The analytical identification performed in [29] stated that the only configuration of first-order or low-pass NGD circuits associated with the series-impedance configuration is an *RC*-parallel network.

$$Z_s(j\omega) = \frac{R_s}{1 + j\omega R_s C_s}. \quad (41)$$

Figure 7 represents the configuration of the elementary low-pass NGD cell.

4.1.1 Frequency-dependent S Parameter and Group Delay

The frequency-dependent S parameter of the proposed impedance-series-type cell can be expressed as

$$\left[S_s(j\omega)\right] = \begin{bmatrix} \dfrac{R_s}{2R_0 + R_s + 2j\omega R_0 R_s C_s} & \dfrac{2R_0\left(j\omega R_s C_s + 1\right)}{2R_0 + R_s + 2j\omega R_0 R_s C_s} \\ \dfrac{2R_0\left(j\omega R_s C_s + 1\right)}{2R_0 + R_s + 2j\omega R_0 R_s C_s} & \dfrac{R_s}{2R_0 + R_s + 2j\omega R_0 R_s C_s} \end{bmatrix} \quad (42)$$

From this we can determine the following reflection-coefficient and insertion-loss magnitudes:

$$\left|S_{s_{22}}(j\omega)\right| = \left|S_{s_{11}}(j\omega)\right| = S_{s_{11}}(\omega)$$

$$= \frac{R_s}{\sqrt{\left(2R_0 + R_s\right)^2 + 4\left(\omega R_0 R_s C_s\right)^2}} \quad (43)$$

$$\left|S_{s_{12}}(j\omega)\right| = \left|S_{s_{21}}(j\omega)\right| = S_{s_{21}}(\omega)$$

$$= \frac{2R_0\sqrt{1+(\omega R_s C_s)^2}}{\sqrt{(2R_0+R_s)^2+4(\omega R_0 R_s C_s)^2}}.$$

The associated transmission phase is given by

$$\varphi_s(\omega) = \arctan(\omega R_s C_s) - \arctan\left(\frac{2\omega R_0 R_s C_s}{2R_0+R_s}\right). \quad (44)$$

From Equation (5), we have the group delay

$$\tau_s(\omega) = \frac{R_s^2 C_s\left(2R_0 R_s^2 C_s^2\omega^2 - 2R_0 - R_s\right)}{\left(1+R_s^2 C_s^2\omega^2\right)\left[(2R_0+R_s)^2+4R_0^2 R_s^2 C_s^2\omega^2\right]} \quad (45)$$

4.1.2 NGD Characterization

At very low frequencies, the *S* parameters of the parallel-impedance-based circuit become

$$\left[S_s(\omega\approx 0)\right] = \begin{bmatrix} \frac{R_s}{2R_0+R_s} & \frac{2R_0}{2R_0+R_s} \\ \frac{2R_0}{2R_0+R_s} & \frac{R_s}{2R_0+R_s} \end{bmatrix}. \quad (46)$$

The associated group delay is given by

$$\tau_s(\omega\approx 0) = \frac{-R_s^2 C_s}{R_s+2R_0}. \quad (47)$$

It can be understood from the previous expression in Equation (47) that the passive cell introduced in Figure 3 behaves as a low-pass NGD circuit. In addition to the previous characteristics, one of the most important properties of the NGD cell is the NGD cutoff frequency, which can be denoted ω_{c_s}. It is the root of the equation $\tau_s(\omega_{c_s}) = 0$. The proposed shunt-impedance-based low-pass NGD-cell cutoff frequency is given by

$$\omega_{c_s} = \frac{\sqrt{1+\frac{R_s}{2R_0}}}{R_s C_s}. \quad (48)$$

The NGD figure-of-merit is expressed as

$$FoM_{low-pass_s} = \frac{-R_s}{(2R_0+R_s)\sqrt{R_s+2R_0}}. \quad (49)$$

In this case, it can be emphasized that the figure-of-merit is proportional to the resistance, R_p.

4.1.3 NGD Synthesis Method

The synthesis method consists of calculating R_s and C_s, which can be determined from the system of Equations (11) by considering the proposed series-impedance-type cell. The synthesis formulas are given by

$$\begin{cases} R_s(S_{11}) = R_s(S_{22}) = \frac{2r}{1-r}R_0 \\ \text{or} \\ R_s(S_{12}) = R_s(S_{21}) = \frac{1-a}{2a}R_0 \end{cases}, \quad (50)$$

$$\begin{cases} C_s(\tau_0) = -\frac{R_s+2R_0}{R_s^2}\tau_0 \\ \text{or} \\ C_s(\omega_c) = \frac{\sqrt{1+\frac{R_s}{2R_0}}}{R_s\omega_c} \end{cases}. \quad (51)$$

In the case of reflection-coefficient-based s_p resistance synthesis, the insertion loss is expressed as a function of *r* by the equation $S_{s_{21}}(\omega\approx 0) = r$. In the case of synthesis from the insertion loss, the reflection coefficient is expressed as a function of *a* by the equation $S_{s_{11}}(\omega\approx 0) = 1-a$.

4.1.4 Equivalence Between the Parallel-and Series-Impedance Low-Pass NGD Cells

The equivalence between the two parallel- and series-impedance-based passive NGD topologies under study presents an electrical equivalence. By comparison of the transmission-parameter expressions, we have the equivalent relationship between the parallel and series resistances expressed as

$$R_p R_s = R_0^2. \quad (52)$$

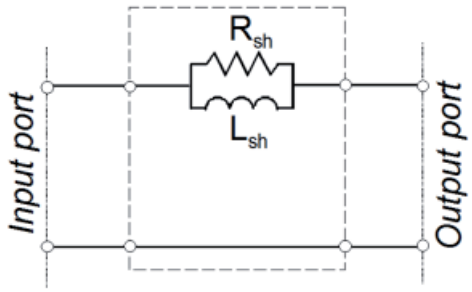

Figure 8. A high-pass NGD cell: *RL*-parallel series network associated with the low-pass cell shown in Figure 7.

In the same manner, the reactive-parameter equivalent relationships can be written as

$$\frac{L_p}{C_s} = R_0^2 . \tag{53}$$

4.2 High-Pass NGD Elementary Cells

The present subsection is focused on the NGD characteristics of the high-pass NGD cell associated with the circuit shown in Figure 7. The corresponding high-pass cell is depicted in Figure 8. The high-pass NGD cell is easily synthesized from the low-pass cell via the low-pass-to-high-pass transform. The resistance element is not changed: $R_{sh} = R_s$.

4.2.1 High-Pass NGD Behavior

The *S* parameters of the series-impedance-based cell shown in Figure 4 become

$$\left[S_{sh}(j\omega)\right] =$$

$$\begin{bmatrix} \dfrac{j\omega R_s L_{sh}}{2R_0R_s + j\omega L_{sh}(2R_0+R_s)} & \dfrac{2R_0(R_s + j\omega L_{sh})}{2R_0R_s + j\omega L_{sh}(2R_0+R_s)} \\ \dfrac{2R_0(R_s + j\omega L_{sh})}{2R_0R_s + j\omega L_{sh}(2R_0+R_s)} & \dfrac{j\omega R_s L_{sh}}{2R_0R_s + j\omega L_{sh}(2R_0+R_s)} \end{bmatrix} \tag{54}$$

The associated group delay is given by

$$\tau_{sh}(\omega \approx 0) = \frac{L_{sh}}{2R_0} . \tag{55}$$

The NGD cutoff frequency, $\omega_{c_{sh}}$, is given by

$$\omega_{c_{sh}} = \frac{R_s\sqrt{2R_0}}{L_{sh}\sqrt{2R_0+R_s}} . \tag{56}$$

Moreover, it is also found that for any integer $n > 1$, the group delay can be expressed as

$$\tau_{sh}\left(\omega = n\omega_{c_{sh}}\right) =$$

$$\frac{\left(1-n^2\right)L_{sh}\left(2R_0+R_s\right)}{\left[2\left(1+n^2\right)R_0+R_s\right]\left[2\left(1+n^2\right)R_0+n^2R_s\right]} . \tag{57}$$

It can be understood from Equation (55), $\tau_{sh}(\omega \approx 0) > 0$, and Equation (57), $\tau_{sh}\left(\omega = n\omega_{c_{sh}}\right) < 0$, which generally means that $\tau_{sh}\left(\omega > \omega_{c_{sh}}\right) < 0$. This means that the passive cell introduced in Figure 8 behaves as a high-pass NGD circuit.

The NGD figure-of-merit is expressed as

$$FoM_{high-pass_s} = FoM_{low-pass_s} , \tag{58}$$

which is proportional to the resistance R_s.

4.2.2 Synthesis Method

The high-pass NGD resistance, $R_{sh} = R_s$, can be synthesized from Equation (50). Given the targeted positive group delay $\tau_0 > 0$, the inductance parameter can be synthesized from the group delay expressed in Equation (55), given by

$$L_{sh} = 2R_0\tau_0 . \tag{59}$$

The high-pass NGD cell inductance can also be alternatively determined from the high-pass cutoff frequency introduced in Equation (57):

$$L_{sh} = \frac{R_s\sqrt{2R_0}}{\omega_{c_{sh}}\sqrt{2R_0+R_s}} . \tag{60}$$

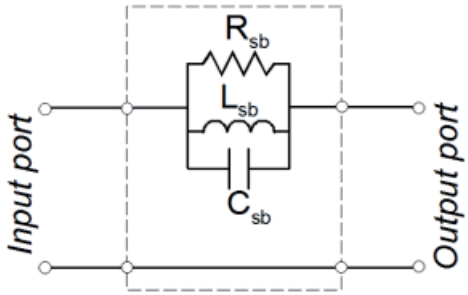

Figure 9. A bandpass NGD cell: *RLC*-parallel series network associated with the low-pass cell shown in Figure 7.

4.3 Bandpass NGD Elementary Cell

In this case, to synthesize the associated bandpass NGD cell we just need to replace the capacitor LC_s by an *LC*-parallel network, and we obtain the elementary cell shown in Figure 9. The resistance element is not changed, $R_{sb} = R_s$.

4.3.1 Bandpass NGD Behavior

The proposed cell's resonance frequency, which is also the NGD central frequency, is defined by

$$\omega_0 = \frac{1}{\sqrt{L_{sb}C_s}}. \tag{61}$$

The NGD bandpass behavior can be understood from the insertion-loss expression. The associated *S* parameters at the center frequency are then expressed as

$$\left[S_{sb}(\omega_0)\right] = \left[S_s(0)\right] = \begin{bmatrix} \frac{R_s}{2R_0 + R_s} & \frac{2R_0}{2R_0 + R_s} \\ \frac{2R_0}{2R_0 + R_s} & \frac{R_s}{2R_0 + R_s} \end{bmatrix} \tag{62}$$

The group delay is given by

$$\tau_{sb}(\omega_0) = 2\tau_s(0) = \frac{-4R_s^2 C_{sb}}{R_s + 2R_0}. \tag{63}$$

4.3.2 Bandpass NGD Characterization and Properties

The NGD center frequency of the passive cell shown in Figure 9 is equal to $\omega = \omega_0$. The NGD bandwidth is defined by

$$\Delta\omega_{c_{sb}} = 2\omega_{c_s} = \frac{\sqrt{1 + \frac{R_s}{2R_0}}}{R_s C_{sb}}. \tag{64}$$

This means that the NGD cutoff frequencies are defined by

$$\omega_{c_{sb}} = \omega_0 \pm \omega_{c_s} = \frac{1}{\sqrt{L_{sb}C_{sb}}} \pm \frac{\sqrt{1 + \frac{R_s}{2R_0}}}{R_s C_{sb}}. \tag{65}$$

This bandpass cell's NGD figure-of-merit is expressed as

$$FoM_{band-pass_s} = 2FoM_{low-pass_s}, \tag{66}$$

which is proportional to the resistance, R_s.

4.3.3 Synthesis Method

Similarly to the previous case of Subsection 3.3.3, the bandpass NGD cell resistance and capacitor parameters can be determined from the associated low-pass cell. The same equation allows determining the resistance. However, two times the low-pass NGD cell capacitor, $C_{sb} = 2C_s$, must be considered, based on the group delay defined in Equation (56). The associated inductance can be calculated from the inductance and the expected NGD center angular frequency, which can be denoted ω_0. We therefore have the synthesis formula

$$L_{sb} = \frac{1}{\omega_0^2 C_{sb}}. \tag{67}$$

4.4 Stop-Band NGD Elementary Cells

Similarly to Subsection 3.4, the stop-band NGD cell can be easily synthesized from the low-pass cells via the

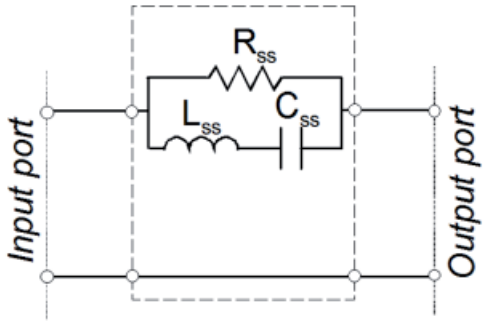

Figure 10. A stop-band NGD cell: *R* and *LC*-series parallel network associated with the low-pass cell shown in Figure 7.

low-pass-to-stop-band transform. Figure 10 represents the configuration of the impedance-series-type stop-band NGD cell. The resistance element is not changed: $R_{ss} = R_s$.

4.4.1 Stop-Band NGD Behavior

The proposed cell's resonance frequency is defined by

$$\omega_0 = \frac{1}{\sqrt{L_{ss}C_{ss}}}. \tag{68}$$

It can be demonstrated that the associated group delay is

$$\tau_{ss}(\omega_0) = \frac{L_{ss}}{2R_0}. \tag{69}$$

This group delay is always positive around the resonance frequency.

4.4.2 Stop-Band NGD Characterization and Properties

The proposed shunt-impedance-based stop-band NGD cell's cut-off frequencies are given by

$$\omega_{c_{ss}} = \frac{1}{\sqrt{L_{ss}C_{ss}}} \pm \frac{R_s\sqrt{2R_0}}{L_{ss}\sqrt{2R_0 + R_s}}. \tag{70}$$

This means that the NGD bandwidths are

$$\begin{cases} \omega \le \dfrac{1}{\sqrt{L_{ss}C_{ss}}} - \dfrac{R_s\sqrt{2R_0}}{L_{ss}\sqrt{2R_0 + R_s}} \\ \text{and} \\ \omega \ge \dfrac{1}{\sqrt{L_{ss}C_{ss}}} + \dfrac{R_s\sqrt{2R_0}}{L_{ss}\sqrt{2R_0 + R_s}}. \end{cases} \tag{71}$$

For the case of the stop-band cell, the figure-of-merit cannot be defined.

4.4.3 Synthesis Method

By analogy with Section 3.4.3, the stop-pass NGD cell-synthesis relationships can be inspired by the combination of the low-pass and high-pass relationships. The resistance is the same relationship as for the low-pass cell defined in Equation (50). The inductance must be the same as for the high-pass cell defined in Equation (59) or Equation (60), $L_{ss} = L_{sh}$. The associated capacitor can be calculated from the inductance and the expected NGD center angular frequency, which can be denoted ω_0. We therefore have the capacitor-synthesis formula

$$C_{ss} = \frac{1}{\omega_0^2 L_{sh}}. \tag{72}$$

To validate the overall NGD circuit theory, the design, simulation, and experiments for low-pass, high-pass, bandpass, and band-stop NGD cells built with lumped *R*, *L*, and *C* based elements are presented in the next section.

5. Validation Results

It can be understood from the previous theory that the NGD circuit under study can be assumed to behave like any familiar electronic circuit. The present section is focused on the simulation results of proof-of-concept NGD cells synthesized from the developed theory. The family of two previously explored topologies based on parallel and series impedances is explored. For each family, the low-pass NGD circuits were synthesized, designed, simulated, fabricated, and tested in order to achieve the following arbitrary specifications:

- NGD level $\tau_0 = -1$ ns
- Reflection coefficient $r = -12$ dB.

The associated following circuits were then synthesized:

Table 2. Synthesized NGD circuit parameters.

Type Of NGD Cells	Low-Pass	High-Pass	Bandpass	Stop-Band
Resistance parameter	$R_p = 74.53\ \Omega$ $R_s = 33.54\ \Omega$			
Inductance parameter	$L_p = 2.97$ nH	$L_{sh} = 100$ nF	$L_{pb} = L_p$ $L_{sb} = 0.85$ nH	$L_{ps} = 2.53$ nH $L_{ss} = L_{sh}$
Capacitor parameter	$C_s = 119$ pF	$C_{ph} = 40$ pF	$C_{pb} = 0.34$ pF $C_{sb} = C_s$	$C_{ps} = C_{ph}$ $C_{sh} = 1.01$ pF

- High-pass NGD cell,
- Bandpass NGD cell aimed at operating at a center frequency of $f_0 = 0.5$ GHz,
- Stop-band NGD cell with a center frequency $f_0 = 0.5$ GHz.

The proof-of-concept modeled computed results were compared with simulations run in the *ADS*® environment of the electronic circuit designer and simulator. The proposed *S*-parameter simulations were performed from dc to 1 GHz. The simulation results obtained will be explored in the next paragraphs.

5.1 NGD Cell Proof-of-Concept Syntheses and Designs

After the circuit synthesis from the arbitrary given NGD and specifications, the NGD circuit examples will be described. The NGD functionality can be understood from the simulations. Table 2 summarizes the parameters of the low-pass, high-pass, bandpass, and stop-band NGD cells synthesized given the specifications $\tau_0 = -1$ ns and $r = -12$ dB.

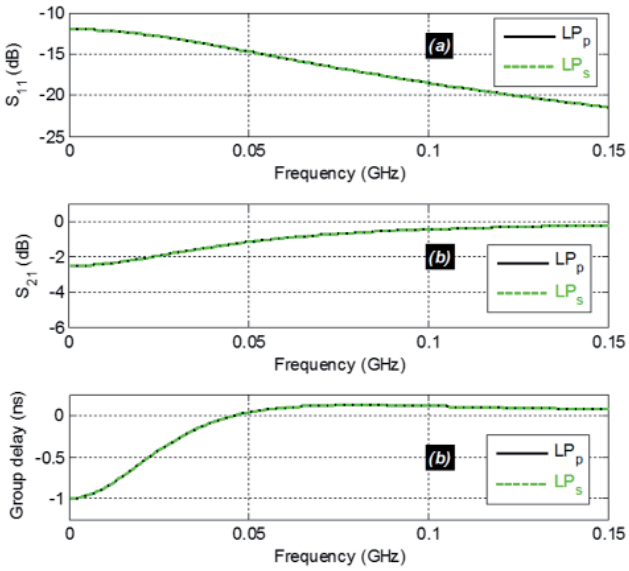

Figure 11. (a) The reflection and (b) transmission coefficients, and (c) group delay of the low-pass NGD circuits shown in Figure 3 and Figure 7.

5.2 Frequency-Domain Results

S-parameter simulations of circuits parameterized as addressed in the first column of Table 2 were performed to illustrate the low-pass, high-pass, bandpass, and stop-band NGD functions.

5.2.1 Low-Pass NGD Results

Figures 11a and 11b respectively display the reflection and transmission coefficients of the low-pass NGD cells shown in Figure 3 and Figure 7 for the shunt- and series-impedance-based topologies. The shunt-impedance-based results are plotted with the solid line, and the series-impedance-based results are plotted with the dashed line. As illustrated by Figure 11c, these passive cells behaved as a low-pass NGD function with the same characteristics. The theoretical prediction and the simulations were in very good agreement, and they confirmed the low-pass NGD function with the proposed passive lumped cells. Both cells generated the same *S*-parameter results. They presented a low-pass NGD level $\tau(0) = -1$ ns and a cutoff frequency of about $f_c(NCD) = 46$ MHz. Over the NGD bandwidth, the insertion loss varied from -2.5 dB to -1.27 dB. In other words, the insertion-loss flatness was about 1.23 dB. The reflection coefficients were better than -12 dB.

5.2.2 High-Pass NGD Results

To simulate the high-pass cells, the parameters of the high-pass cells shown in Figure 4 (for the parallel-impedance-based cell) and in Figure 8 (for the series-impedance-based cell) addressed in the second column of Table 1 were considered. Figures 12a and 12(b) respectively display the reflection- and transmission-coefficient plots. Figure 12c depicts the associated group delays. As expected, both cells generated the same *S*-parameter results. In addition, they behaved as having an NGD high-pass

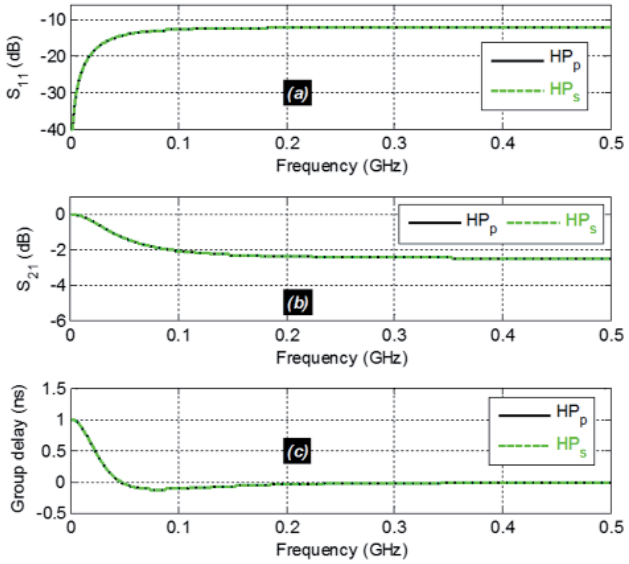

Figure 12. (a) The reflection and (b) transmission coefficients, and (c) the group delay of the high-pass NGD circuits shown in Figure 4 and Figure 8.

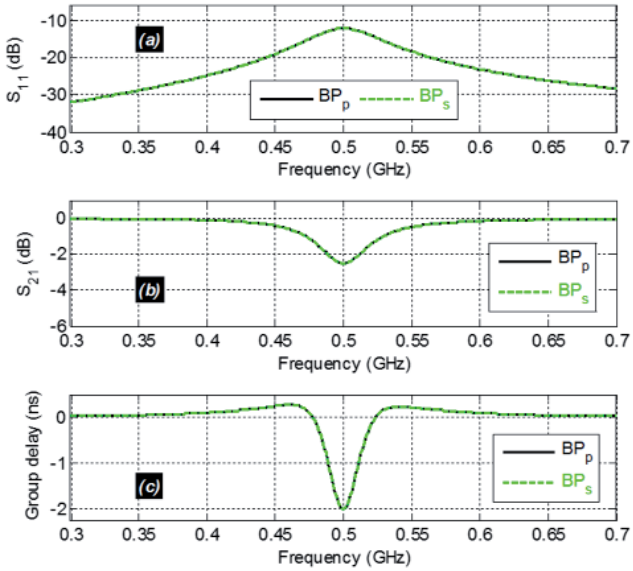

Figure 13. (a) The reflection and (b) transmission coefficients, and (c) the group delay of the bandpass NGD circuits shown in Figure 5 and Figure 9.

function. As theoretically predicted, the high-pass group delay, $\tau_{hp}(f) = -\tau_{lp}(f)$ was the opposite of the low-pass group-delay frequency response. It can be emphasized that the group delay was positive when $f < f_c$ and negative when $f > f_c$. A very good correlation between the theoretical concept of the high-pass NGD function and the simulations was obtained. As seen in Figure 12b, the insertion loss varied from -2.38 dB to -1.25 dB over the NGD bandwidth. The reflection coefficients were better than -12 dB.

5.2.3 Bandpass NGD Results

To illustrate the feasibility of the bandpass NGD function, the parameters of the cells introduced in Figure 5 (for the parallel-impedance-based cell) and in Figure 9 (for the series-impedance-based cell) defined in the third column of Table 1 were considered. The simulated reflection and transmission parameters from 0.3 GHz to 0.7 GHz were respectively plotted in Figures 13a and 13b. Both cells presented similar *S*-parameter responses. More importantly, Figure 13c presents the group-delay frequency responses of the simulated circuits. As predicted in theory, the proposed lumped cells behaved with a bandpass NGD function. The cells generated NGD with level $\tau(f_0) = -2$ ns at the specified center frequency $f_0 = 0.5$ GHz. The NGD bandwidth was about $\Delta f_{NGD} = 92$ MHz. In the NGD bandwidth, the insertion loss varied from -2.5 dB to -1.27 dB. In other words, the insertion loss flatness was about 1.23 dB. The bandpass NGD cell reflection coefficients were better than -12 dB.

5.2.4 Stop-Band NGD Results

The stop-band NGD circuits shown in Figure 6 (for the parallel-impedance-based cell) and Figure 10 (for the series-impedance-based cell) were simulated with the parameters indicated in the last column of Table 1. The simulated reflection and transmission parameters are respectively displayed in Figures 14a and 14b. Both cells presented the same frequency responses. The group-delay responses are plotted in Figure 14c. As expected in theory, the circuit generated the NGD stop-band function. The stop-band NGD circuit group-delay frequency response $\tau_{sb}(f) = -\tau_{bp}(f)$ was the opposite of the bandpass NGD circuit's response. The group delay was positive in the frequency band centered at $f_0 = 0.5$ GHz with a bandwidth of about $\pm\Delta f_{NGD}/2 = 46$ MHz. As seen in Figure 14b, the insertion loss varied from -2.38 dB to -1.25 dB in the NGD bandwidth. The reflection coefficients are better than -12 dB.

5.3 Illustrative Time-Domain Results

In addition to this frequency-domain analysis introduced in the previous subsection, a time-domain investigation was also performed. The results reported in the present subsection are constrained only to the low-pass NGD cells. The proposed time-domain investigation was carried out with the *ADS*® transient analyses in the time parameters $t_{\min} = 0$ and $t_{\max} = 50$ ns with a time step of $\Delta t = 0.2$ ns. Figure 15 shows the configuration of the simulated circuits.

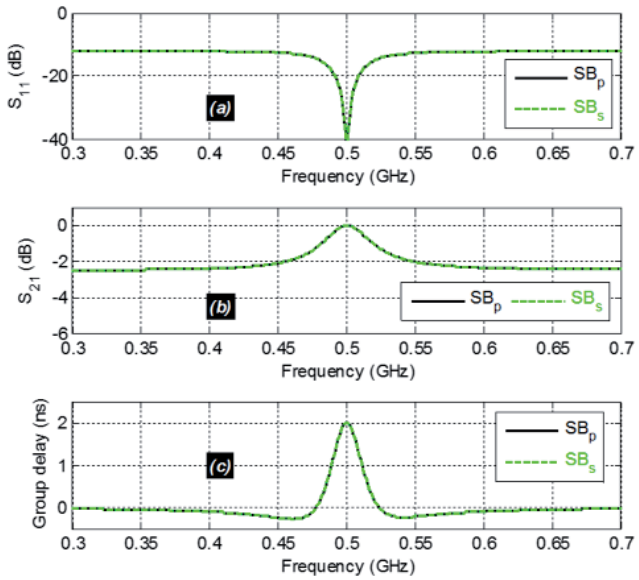

Figure 14. (a) The reflection and (b) transmission coefficients, and (c) the group delay of the stop-band NGD circuits shown in Figure 6 and Figure 10.

Three different input test voltages were attributed to v_{in} : v_1 (a Gaussian signal with a full width of about 40 ns), and arbitrary-waveform signals v_2 and v_3 . Figure 16 presents the plots of the comparisons of the transient input and output voltages generated by the parallel-impedance- and series-impedance-based low-pass NGD cells. The input signals were plotted in dotted lines. The shunt-impedance-based cell outputs were plotted with solid lines, and the series-impedance-based cell outputs were plotted with dashed lines. For the three different cases as seen in Figures $16a_1$, $16a_2$ and $16a_3$, the output-voltage signals were significantly attenuated. However, it could be understood from the comparative plots of normalized voltages shown in Figures $16b_1$, $16b_2$, and $16b_3$ that the time advances induced by the NGD phenomena were generated for the different waveform test signals.

The time advance could be assessed with the time shift between the minimum and maximum peaks of the input and output transient signals. This effect can be generated only for the baseband signal presenting a significant spectral frequency band belonging to the NGD bandwidth. Because of the non-flat nature of the group-delay responses shown in Figure 11b over the NGD bandwidth, the time advance could be evaluated from -1 ns to -0.4 ns as a function of the input signal time slope.

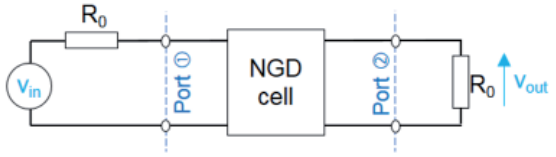

Figure 15. The configuration of the time-domain simulated circuits.

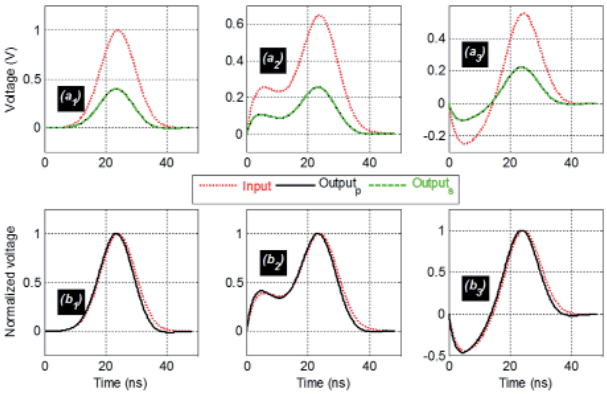

Figure 16. The time-domain simulation results for the low-pass NGD circuit shown in Figure 3 and Figure 7 for three different input signals: (a_1) v_1 , (a_2) v_2 , and (a_3) v_3 , and the associated normalized results: (b_1) v_1 (b_2) v_2 , and (b_3) v_3 .

6. Conclusion

A basic theory for understand the NGD function has been proposed. The fundamental knowledge enabling familiarization with NGD circuit design was described. More practically, a general RF circuit theory for passive NGD topologies was developed. Two types of topologies, based on the *R*, *L*, and *C* lumped-element parallel- and series-impedances, were investigated. For each topology, the *S*-parameter models were established, and the elementary low-pass NGD cell was identified. The NGD behavior, characterization, properties, and synthesis methods were then explained. The associated high-pass, bandpass, and stop-band cells were also investigated. The theoretical concepts were validated with proof-of-concept designs and simulations. Very good agreement between the theory and simulation results was found. As expected from the theory, the low-pass circuits generated NGD levels of about -1 ns over a bandwidth of about 46 MHz. The bandpass prototypes were synthesized to operate around a NGD center frequency of around 0.5 GHz. The high-pass NGD cell generated a group delay equal to the opposite of the low-pass cell. The bandpass NGD function was obtained with a NGD level of about -2 ns, centered at 0.5 GHz. Finally, transient simulations illustrated the time-advance effect caused by the NGD low-pass phenomenon.

7. Reference

1. C. G. B. Garrett and D. E. McGumber "Propagation of a Gaussian Light Pulse Through an Anomalous Dispersion Medium," *Phys. Rev. A*, **1**, 2, 1970, pp. 305-313.

2. S. Chu and S. Wong, "Linear Pulse Propagation in an Absorbing Medium," *Phys. Rev. Lett.*, **48**, 11, 1982, pp. 738-741.

3. R. Y. Chiao, "Atomic Coherence Effects Which Produce Superluminal (But Causal) Propagation of Wavepackets," *Quantum Optics: Journal of the European Optical Society Part B*, **6**, 4, 1994, pp. 359-369.

4. R. Y. Chiao, E. L. Bolda, J. Bowie, J. Boyce, and M. W. Mitchell, "Superluminality and Amplifiers," *Prog. Crystal Growth Charact. Mat*., **33**, 1996, pp. 319-325.

5. M. W. Mitchelll, and R. Y. Chiao, "Causality and Negative Group Delays in a Simple Bandpass Amplifier," *Am. J. Phys.*, **66**, 14, 1998, pp. 14-19.

6. M. W. Mitchell, and R. Y. Chiao, "Negative Group Delay and 'Fronts' in a Causal System: An Experiment With Very Low Frequency Bandpass Amplifiers," *Phys. Lett. A*, **230**, June 1997, pp. 133-138.

7. L. J. Wang, A. Kuzmich and A. Dogariu, "Gain-Assisted Superluminal Light Propagation," *Nature*, **406**, June 2000, pp. 277-279.

8. A. Dogariu, A. Kuzmich, H. Cao and L. J. Wang, "Superluminal Light Pulse Propagation via Rephasing in a Transparent Anomalously Dispersive Medium," *Optics Express*, **8**, 6, Mar. 2001, pp. 344-350.

9. H. Cao, A. Dogariu, and L. J. Wang, "Negative Group Delay and Pulse Compression in Superluminal Pulse Propagation," *IEEE Journal of Selected Topics in Quantum Electronics*, **9**, 1, February 2003, pp. 52-58.

10. M. Kitano, T. Nakanishi, K. Sugiyama, "Negative Group Delay and Superluminal Propagation: An Electronic Circuit Approach," *IEEE Journal of Selected Topics in Quantum Electronics*, **9**, 1, 2003, pp. 43-51.

11. T. Nakanishi, K. Sugiyama, and M. Kitano, "Demonstration of Negative Group Delays in a Simple Electronic Circuit," *Am. J. Phys.*, **70**, 11, 2002, pp. 1117-1121.

12. J. N. Munday, and R. H. Henderson, "Superluminal Time Advance of a Complex Audio Signal," *Appl. Phys. Lett.*, **85**, July 2004, pp. 503-504.

13. S. Lucyszyn, and I. D. Robertson, "Analog Reflection Topology Building Blocks for Adaptive Microwave Signal Processing Applications," *IEEE Trans. Microwave Theory Techn*., **43**, 3, 1995, pp. 601-611.

14. S. Lucyszyn, I. D. Robertson and A.H. Aghvami, "Negative Group Delay Synthesizer," *Electronics Letters*, **29**, 9, April 1993, pp. 798-800.

15. C. D. Broomfield and J. K. A. Everard, "Broadband Negative Group Delay Networks for Compensation of Oscillators Using Feedforward Amplifiers," *Electronics Letters*, **36**, 23, September 2000, pp. 1710-1711.

16. G. V. Eleftheriades, O. Siddiqui, and A. K. Iyer, "Transmission Line Models for Negative Refractive Index Media and Associated Implementations Without Excess Resonators," *IEEE Microwave Wireless Component Letters*, **13**, 2, February 2003, pp. 51-53.

17. O. F. Siddiqui, M. Mojahedi and G. V. Eleftheriades, "Periodically Loaded Transmission Line With Effective Negative Refractive Index and Negative Group Velocity," *IEEE Trans. Antennas Propagat*., **51**, 10, Oct. 2003, pp. 2619-2625.

18. O. F. Siddiqui, S. J. Erickson, G. V. Eleftheriades, M. Mojahedi, "Time-Domain Measurement of Negative Group Delay in Negative-Refractive-Index Transmission-Line Metamaterials," *IEEE Trans. Microwave Theory Techn.*, **52**, 5, May 2004, pp. 1449-1454.

19. N. S. Bukhman, and S. V. Bukhman, "On the Negative Delay Time of a Narrow-Band Signal as It Passes Through the Resonant Filter of Absorption," *Radiophysics and Quantum Electronics*, **47**, 1, 2004, pp. 66-76.

20. S. S. Oh and L. Shafai, "Compensated Circuit with Characteristics of Lossless Double Negative Materials and Its Application to Array Antennas," *IET Microw. Antennas Propag*., **1**, 1, February 2007, pp. 29-38.

21. H. Choi, Y. Jeong, J. Lim, S. Y. Eom, Y. B. Jung, "A Novel Design for a Dual-Band Negative Group Delay Circuit," *IEEE Microwave Wireless Component Letters*, **21**, 1, January 2011, pp. 19-21.

22. G. Chaudhary and Y. Jeong, "Tunable Center Frequency Negative Group Delay Filter Using Coupling Matrix Approach," *IEEE Microwave Wireless Component Letters*, **27**, 1, 2017, pp. 37-39.

23. G. Liu, and J. Xu, "Compact Transmission-Type Negative Group Delay Circuit with Low Attenuation," *Electronics Letters*, **53**, 7, March 2017, pp. 476-478.

24. W. Alomar and A. Mortazawi, "Method of Generating Negative Group Delay in Phase Arrays Without Using Lossy Circuits," *Proc. IEEE Int. Wireless Symp. (IWS) 2013*, Beijing, China, 14-18 April 2013, pp. 1-4.

25. B. Ravelo, "Investigation on Microwave Negative Group Delay Circuit," *Electromagnetics*, **31**, 8, November 2011, pp. 537-549.

26. B. Ravelo, "Methodology of Elementary Negative Group Delay Active Topologies Identification," *IET Circuits Devices Syst. (CDS)*, **7**, 3, May 2013, pp. 105-113.

27. C.-T. M. Wu and T. Itoh, "Maximally Flat Negative Group Delay Circuit: A Microwave Transversal Filter Approach," *IEEE Trans. on Microwave Theory and Techniques*, **62**, 6, June 2014, pp. 1330-1342.

28. B. Ravelo, "Demonstration of Negative Signal Delay with Short-Duration Transient Pulse," *Eur. Phys. J. Appl. Phys. (EPJAP)*, **55** (10103), 2011, pp. 1-8.

29. B. Ravelo, "Similitude Between the NGD Function and Filter Gain Behaviours," *Int. J. Circ. Theor. Appl.*, **42**, 10, October 2014, pp. 1016-1032

30. B. Ravelo, "High-Pass Negative Group Delay RC-Network Impedance," *IEEE Transactions on Circuits and Systems II: Express Briefs*, **64**, 9, September 2017, pp. 1052-1056.

31. M. Kandic and G. E. Bridges, "Asymptotic Limits of Negative Group Delay in Active Resonator-Based Distributed Circuits," *IEEE Transactions on Circuits and Systems I: Regular Papers*, **58**, 8, August 2011, pp. 1727-1735.

32. P. K. Chan and K. Karplus, "Computing Signal Delay in General RC Networks by Tree/Link Partitioning," *IEEE Trans. Computed Aided Design*, **8**, 9, August 1990, pp. 898-902.

33. R. Y. Chiao, "Faster Than Light Propagations, Negative Group Delays, and their Applications," *The Physics of Communication Proc. of the XXII Solvay Conference on Physics*, DOI 10.1142, November 2001, pp. 287-314.

34. D. Solli, R. Y. Chiao, and J. M. Hickmann, "Superluminal Effects and Negative Delays in Electronics, and their Applications," *Phys. Rev. E*, **66**, 5, November 2002, pp. 056601.1-056601.4.

35. B. Ravelo and A. K. Jastrzebski, "NGD Circuit Using a Microwave Amplifier for the Signal Integrity Improvement," Proc. of 2012 Asia-Pacific Symposium on Electromagnetic Compatibility (APEMC 2012), Singapore, 21-24 May 2012, pp. 1-4.

36. B. Ravelo, "Recovery of Microwave-Digital Signal Integrity with NGD Circuits," *Photonics and Optoelectronics (P&O)*, **2**, 1, January 2013, pp. 8-16.

37. B. Ravelo, S. Lalléchère, A. Thakur, A. Saini and P. Thakur, "Theory and circuit modelling of Baseband and Modulated Signal Delay Compensations with Low- and Band-Pass NGD Effects," *Int. J. Electron. Commun. (AEÜ)*, **70**, 9, September 2016, pp. 1122-1127.

38. H. Choi, Y. Jeong, C. D. Kim, and J. S. Kenney, "Efficiency Enhancement of Feedforward Amplifiers by Employing a Negative Group Delay Circuit," *IEEE Trans. Microw. Theory Tech.*, **58**, 5, May 2010, pp. 1116-1125.